Conversion of Abandoned Property to Green Space as a Strategy to Mitigate the Urban Heat Island Investigated with Numerical Simulations

TIMOTHY J. CADY,[a,c] DAVID A. RAHN,[a] NATHANIEL A. BRUNSELL,[a] AND WARD LYLES[b]

[a] *Department of Geography and Atmospheric Science, University of Kansas, Lawrence, Kansas;* [b] *Urban Planning Program, School of Public Affairs and Administration, University of Kansas, Lawrence, Kansas*

(Manuscript received 14 April 2020, in final form 29 August 2020)

ABSTRACT: Impervious surfaces and buildings in the urban environment alter the radiative balance and surface energy exchange and can lead to warmer temperatures known as the urban heat island (UHI), which can increase heat-related illness and mortality. Continued urbanization and anthropogenic warming will enhance city temperatures worldwide, raising the need for viable mitigation strategies. Increasing green space throughout a city is a viable option to lessen the impacts of the UHI but can be difficult to implement. The potential impact of converting existing vacant lots in Kansas City, Missouri, to green spaces is explored with numerical simulations for three heat-wave events. Using data on vacant property and identifying places with a high fraction of impervious surfaces, the most suitable areas for converting vacant lots to green spaces is determined. Land-use/land-cover datasets are modified to simulate varying degrees of feasible conversion of urban to green spaces in these areas, and the local cooling effect using each strategy is compared with the unmodified simulation. Under more aggressive greening strategies, a mean local cooling impact of 0.5°–1.0°C is present within the focus area itself during the nighttime hours. Some additional cooling via the ''park cool island'' is possible downwind of the converted green spaces under the more aggressive scenarios. Although moderate and conservative strategies of conversion could still lead to other benefits, those strategies have little impact on cooling. Only an aggressive approach yields significant cooling.

KEYWORDS: Heat islands; Atmosphere-land interaction; Numerical analysis/modeling; Urban meteorology

1. Introduction

As urbanization and anthropogenic global warming continue to increase over the next several decades, their impacts will present many societal challenges. When natural land cover is replaced by urban surfaces, negative impacts on the ecological systems on which society depends occur, including drastic changes to the local surface radiative balance and energy exchange (Randolph 2012; Stone 2012). These energy balance changes reduce evapotranspiration while increasing sensible heat flux (Oke 1988; Taha 1997; Arnfield 2003). Consequently, cities tend to exhibit higher temperatures (e.g., Oke 1995; Tran et al. 2006; Imhoff et al. 2010; Peng et al. 2011; Monaghan et al. 2014; Azevedo et al. 2016) when compared to their rural surroundings, a phenomenon known as the urban heat island (UHI; Oke 1982). UHIs are magnified by anthropogenic processes, most notably from the use of air conditioning systems and emissions from vehicles and industrial activity (Shahmohamadi et al. 2011; Salamanca et al. 2014).

Various strategies can mitigate the impact of anthropogenic warming and widespread urbanization (Akbari et al. 2016). Stone conceptualizes three main sets of strategies: 1) modifying ''physical characteristics of cities to reflect or dissipate heat energy through enhanced surface reflection and vegetative cover,'' 2) addressing ''regional drivers of urban-scale warming through restoring the ecological integrity of metropolitan hinterlands,'' and 3) emphasizing ''energy conservation and efficiency to minimize the production of waste heat in cities'' (Stone 2012, 173–174). We use a slightly modified conceptualization that distinguishes between strategies focused on 1) modifications to constructed elements of the built environment, like buildings and gray infrastructure, or 2) modifications to the natural environment, like vegetation and green infrastructure. In the first category, altering the thermal properties and absorptivity of the built environment, including impervious urban surfaces and building materials, can diminish the intensity of the UHI without making drastic changes to land use/land cover (LULC). Examples include increasing the reflectively of pavement and asphalt by adding specialized materials during production, using reflective paints and sealants to increase albedo, and implementing color-changing surfaces that adapt to the diurnal radiation cycle (Takebayashi and Moriyama 2007; Susca et al. 2011). Increasing the permeability of surface materials can increase moisture availability and thus evapotranspiration rates (Santamouris 2013). Green roofs replace conventional roofing with vegetation and act to increase surface albedo and enhance evapotranspiration (Santamouris 2014).

In the second category, preservation or restoration of open space and natural vegetation in urban and suburban areas offers the potential to drastically reduce the effects of the UHI (Hart and Sailor 2009; Stone 2012). Observational studies (e.g., Oliveira et al. 2011; Declet-Barreto et al. 2013; Feyisa et al. 2014; Wesley and Brunsell 2019) have demonstrated a significant ''park cool island'' effect associated with urban green spaces of varying sizes and configurations, with cooling impacts often extending into nonvegetated areas. Preserving open spaces and natural vegetation provides additional environmental benefits, including protecting water quality, maintaining biodiversity, mitigating floods, and cleaning the air (Stone 2012; Boswell et al. 2019). These ecosystem services can

[c] Current affiliation: National Weather Service, Houston/Galveston Forecast Office, Dickinson, Texas.

Corresponding author: David A. Rahn, darahn@ku.edu

DOI: 10.1175/JAMC-D-20-0093.1

contribute to public health, enhance land values, and reduce the need for costly gray infrastructure.

An opportunity for UHI reduction also lies with greening urban spaces that have been degraded from a more natural state to unused or underused impervious surfaces (Stone 2012; Boswell et al. 2019). The most promising of these spaces include vacant or abandoned lots and areas excessively dedicated to vehicle parking, though underused roads and even monoculture suburban lawns should be considered as well (Stone 2012). Depending on the size and arrangement of the areas targeted, greening can transform degraded areas into spaces for parks, native habitat, and even small-scale agriculture, generating many of the same benefits as preserving existing green infrastructure and ecosystem services (Randolph 2012; Boswell et al. 2019). For cities and regions with declining populations like the Rust Belt (or even major shifts in land-use patterns within a city or region like in the Sun Belt), major amounts of acreage may be available for greening with minimal displacement or disruption for residents or businesses. These benefits are exemplified by cities like Detroit, which has undertaken a widespread effort to promote the incorporation of green infrastructure and urban farming into redevelopment plans, particularly in areas with widespread swaths of vacant land (Colasanti et al. 2012; Meerow and Newell 2017).[1]

While a major greening program of vacant land is politically and economically infeasible to test on a widespread scale in any city at this time, the development of high-resolution weather models in recent years allows for a detailed numerical simulation of the UHI that can test the temperature response to imposed changes to land use (Chen et al. 2011). The goal of this work is to utilize numerical model simulations to determine the potential impacts of urban greening through realistic land-use conversion scenarios. The greening scenario is based on identifying existing locations of abandoned property in a case study region selected to provide generalizable insights. The simulations allow quantification of the potential impact for mitigating UHIs by converting abandoned properties during extreme heat events and assessing the cooling benefits resulting from conversion of vacant areas to vegetation. The findings can inform planners interested in broadening the array of ecosystem services that can be reliably modeled and used in land-use decision-making.

2. Methods

a. Overview of region

The area of focus is the Kansas City, Missouri, metropolitan area, a midsized temperate city that can experience significant heat waves and contains areas with high amounts of vacant space. Approximately 2.1 million people live along the northern Kansas–Missouri border (U.S. Census Bureau 2018). The region exhibits diverse LULC with a densely populated urban center of Kansas City (population 488 943) that is surrounded by areas of suburban sprawl: low-density suburban development and expansive peripheral areas of cropland, forests, and pastures (Fig. 1a). Kansas City and its surroundings have experienced robust growth in recent years, increasing in population by approximately 16% since 2000 (U.S. Census Bureau 2011). Furthermore, the area's midlatitude inland location has made it prone to prolonged heat waves, most notably including an event in 1980 that was responsible for a 65% increase in mortality (Jones et al. 1982).

The urban core of Kansas City is a strong candidate for large-scale urban greening that could counter the current and expected impacts of the UHI. Like many other locations across the central United States, some parts of the city have suffered from high rates of vacant land and abandoned buildings brought on by the combined forces of population loss, economic disinvestment, and racial segregation during the mid-twentieth century (Pagano and Bowman 2000; L'Heureux 2015). The 2010 U.S. Census shows that high vacancy rates persist across portions of Kansas City despite recent revitalization efforts, particularly in its southeastern portion along the corridor to the east of Troost Avenue (Fig. 1b). The Troost Avenue corridor, described as "one of the primary symbols in Kansas City of disinvestment and racial and economic segregation from the 1950's to today", has lower socioeconomic status and diminished property values compared to surrounding portions of the metropolitan region (Mid-America Regional Council 2013). Historical disinvestment further manifests itself throughout the area through public health inequities, which has been identified as a hot spot for elevated asthma-related hospital visits, low birth weights, and decreased overall life expectancy (City of Kansas City, Division of Community Engagement, Policy and Accountability 2017).

Using block-level data from the 2010 U.S. Census, a region consisting of mostly single-family residential neighborhoods (Mid-America Regional Council 2013) extending eastward from the Troost Avenue corridor could potentially be well-suited for substantial LULC conversion (Fig. 1b). Within the chosen focus area, 5589 of a total of 19 893 residential units are classified as vacant, giving an overall rate of approximately 28%. Considering the greater region's history and high rate of vacant structures, the implementation of widespread urban greening within this focus area has the potential to reduce ambient temperatures during heat-wave events while also addressing the unequal structural systems that have shaped its past development.

b. Numerical simulations of the UHI

Recent advances in computational capabilities permit the UHI and its response to changes in land cover, building properties, and surface materials to be simulated with high-resolution numerical weather models. This is possible due to the development of advanced urban parameterization schemes and high-resolution mapping of urban characteristics that are

[1] At the same time, a cautionary note must be struck because a tension exists between these types of benefits—which can improve quality of life for residents in areas with lots of vacant lands, who are often marginalized and impoverished (Schilling and Logan 2008; Heckert and Mennis 2012)—and the reality that increasing green space often attracts investment capital and leads to gentrification and residents being priced out of their historically neglected neighborhoods.

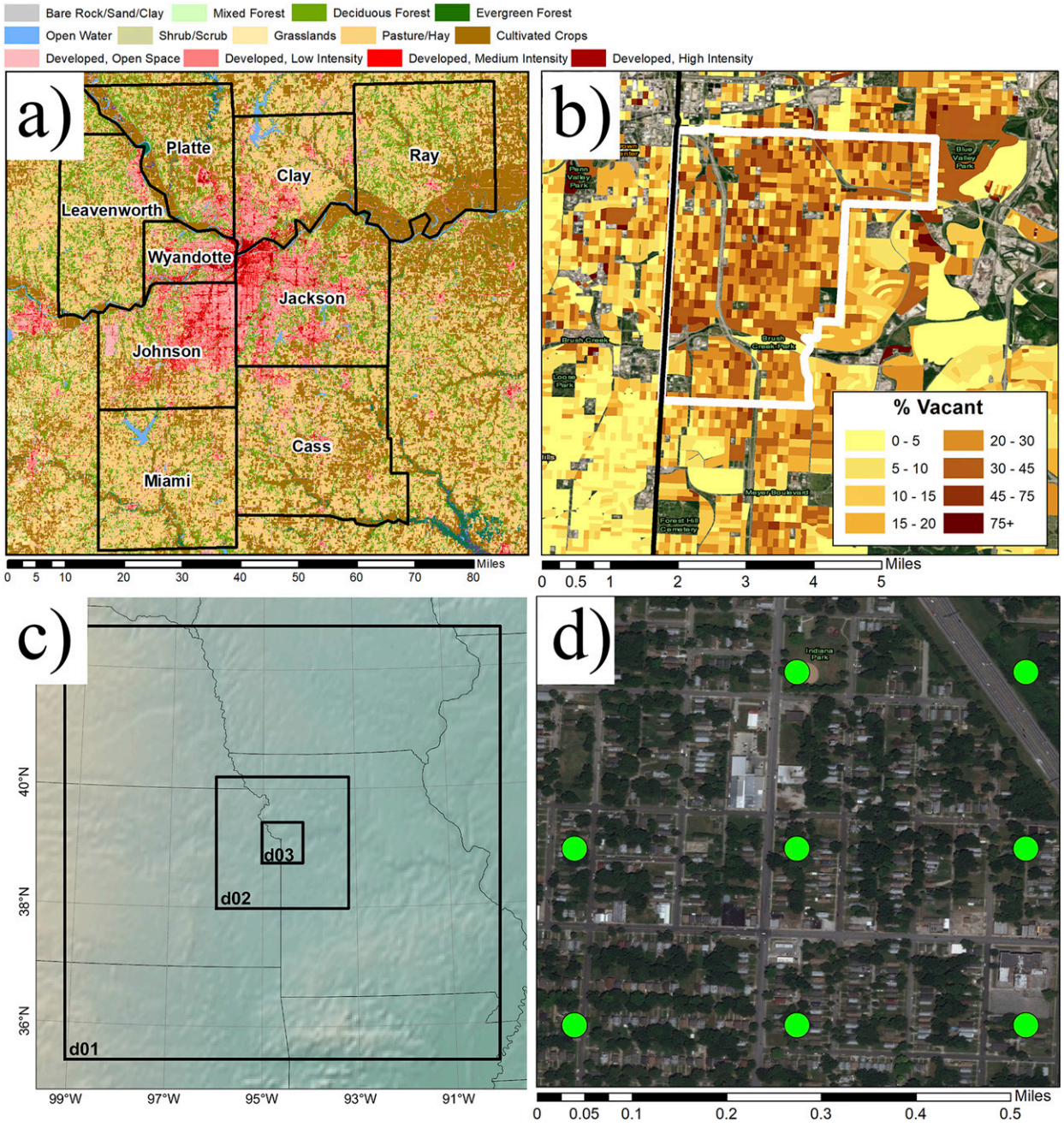

FIG. 1. (a) NLCD land-use categories (shaded) with key above and surrounding counties, (b) vacancy rates (shaded; percent), Troost Avenue (black line), and the focus area (white line), (c) nested model domain boundaries (black), and (d) example of grid spacing (green circles) of d03.

incorporated into models such as the Weather Research and Forecasting (WRF) Model (Skamarock et al. 2005). The ability of WRF to represent the behavior of UHIs at fine scales is thoroughly documented (Chen et al. 2011), and the model has been widely used to examine the mesoscale response of urban temperatures to changes in LULC and variations in anthropogenic activity (e.g., Li and Norford 2016; Fu and Weng 2017; Giannaros et al. 2018).

Previous research has been largely focused on modifying surface material, building properties, and anthropogenic emissions in the existing urban environment to assess the utility of UHI mitigation strategies (e.g., Zhou and Shepherd 2010; Salamanca et al. 2012; Morini et al. 2016). Studies of green space implementation have been more limited. Some recent studies (e.g., Fu and Weng 2017; Giannaros et al. 2018) simulate the response of the UHI to projected changes of LULC

and greening scenarios. However, additional simulations across a diverse set of locations are needed to quantify the impact of planning and land-use strategies on worldwide UHI mitigation, and we employ a more feasible approach here by restricting our conversion to existing vacant lots.

1) WRF CONFIGURATION

WRF (version 4.0.1) is configured similar to previous UHI modeling efforts (e.g., Salamanca et al. 2012; Gutiérrez et al. 2015) and uses three nested grids at horizontal grid spacings of 7.5 km (d01), 1.5 km (d02), and 0.3 km (d03) and grid sizes of 108 × 108, 164 × 164, and 254 × 254 points, respectively (Fig. 1c). There are 82 vertical levels for all domains, spaced more finely near the surface. The innermost model domain encompasses the full extent of Kansas City at approximately block-level scale, with the 300-m grid spacing providing greater detail than in other comparable modeling studies (Fig. 1d). To ensure that the study region was far enough away from the influence of the domain boundaries, the same WRF configuration was used but with larger sizes of all domains. After comparing model output from the different domains, we concluded that the domain sizes used here were sufficiently large. Subsequent analysis uses output from d03 only.

The WRF Preprocessing System (WPS) interpolates meteorological and geographic datasets to the model grids. The simulations are initialized using the National Centers for Environmental Prediction's (NCEP) North American Mesoscale Forecast System analysis (NAM-ANL). During the simulation, only the lateral boundaries of the outermost domain are updated by using the 3-hourly NAM-ANL along the boundaries to nudge the next four points of the outermost domain. Three high-resolution geographic datasets are ingested into WPS to obtain a detailed representation of LULC and urban morphology characteristics that can be modified to reflect different urban greening scenarios. LULC data were acquired from the 2011 National Land Cover Database (NLCD) Land Cover product, a 30-m categorical land-use classification derived from Landsat Thematic Mapper data (Homer et al. 2015). Additional products in the NLCD provide estimates of impervious surface coverage and tree canopy fraction. Elevation data are from the 30-arc-s U.S. Geological Survey (USGS) 2010 Global Multi-Resolution Terrain Elevation dataset (Danielson and Gesch 2011). Detailed urban statistics (e.g., building height distributions, street canyon width) are obtained from the National Urban Data and Access Portal Tool (NUDAPT), which are used to calculate morphology parameters such as surface roughness length and sky-view factor (Glotfelty et al. 2013).

Given that the geographic datasets are higher resolution than the 300-m grid spacing in d03, they must be upscaled and interpolated to the model domain by WPS. The interpolation of surface elevation, for example, is a simple average of all the source data points that are nearer to the center of a model grid cell than to the center of any other model grid cell. More detailed variation in LULC is retained by including the distribution of raw data points within each model grid cell as an array of fractional values for each land-use category (LANDUSEF). Land surface characteristics for the model grid are calculated using these arrays and an associated lookup table containing parameters from the NLCD dataset. It is thus possible to capture the impact of subgridscale variability in LULC across the Kansas City area without requiring model simulations at an inordinately finescale. Similarly, interpolated grids are also constructed from the geographic data for fractional impervious surface area (IMPERV), fractional green area (GREENFRAC), total urban fraction (FRCURB2D), tree canopy fraction (CANFRA), and the 132 urban morphology parameters obtained from the NUDAPT product (URBPARAM).

WRF includes many parameterization schemes that represent subgrid atmospheric processes that cannot be explicitly resolved without prohibitively high computational expense. Urban canopy models (UCMs) of varying complexities have been implemented into WRF, ranging from a simplified bulk parameterization to complex multilayer canopy models that take into account detailed urban morphology characteristics, building material parameters, and anthropogenic heat release (Chen et al. 2011). Considering the importance of these processes in the development of UHIs, the choice of these settings is a critical factor in producing simulations representative of the real atmosphere. However, no single configuration has been determined to best resolve UHIs across all different locations and climates. It is therefore necessary to conduct a series of validation tests to determine the choice of physics settings most suited for simulating the Kansas City UHI before using the model to determine impacts of modifying green spaces.

2) MODEL SYSTEM VALIDATION

Two UCMS are integrated into WRF to represent the impacts of the built environment. The single-layer urban canopy model (SLUCM) is the simpler of the two options, but it has achieved widespread use in WRF analyses of the ability of green spaces to cool urban areas (e.g., Papangelis et al. 2012; Giannaros et al. 2018). SLUCM characterizes the urban canopy layer as a single two-dimensional column, and it includes mass and energy exchanges between the lower atmosphere and the canopy's roof, wall, and street surfaces (Kusaka et al. 2001). Street canyons are parameterized as infinitely long with variable orientation angles and building heights, widths, and thermal characteristics are included to reflect heterogeneous urban morphology. This allows for the effects of shadows, radiation trapping, and diurnal changes in the solar azimuth angle to be considered in calculations of radiative transfer.

A more complex UCM is the building effect parameterization (BEP), which characterizes the three-dimensional structure of mass and momentum transport across multiple layers of the urban canopy (Martilli et al. 2002). By considering the radiative effects of both horizontal and vertical building and street surfaces, BEP is able to more explicitly capture the generation of turbulent kinetic energy within the canopy and its mixing via wake diffusion. BEP is typically coupled with the building energy model (BEM), which parameterizes energy exchange between building interiors and the surrounding environment (Salamanca et al. 2010). BEM accounts for the effects of ventilation, building occupancy, energy consumption,

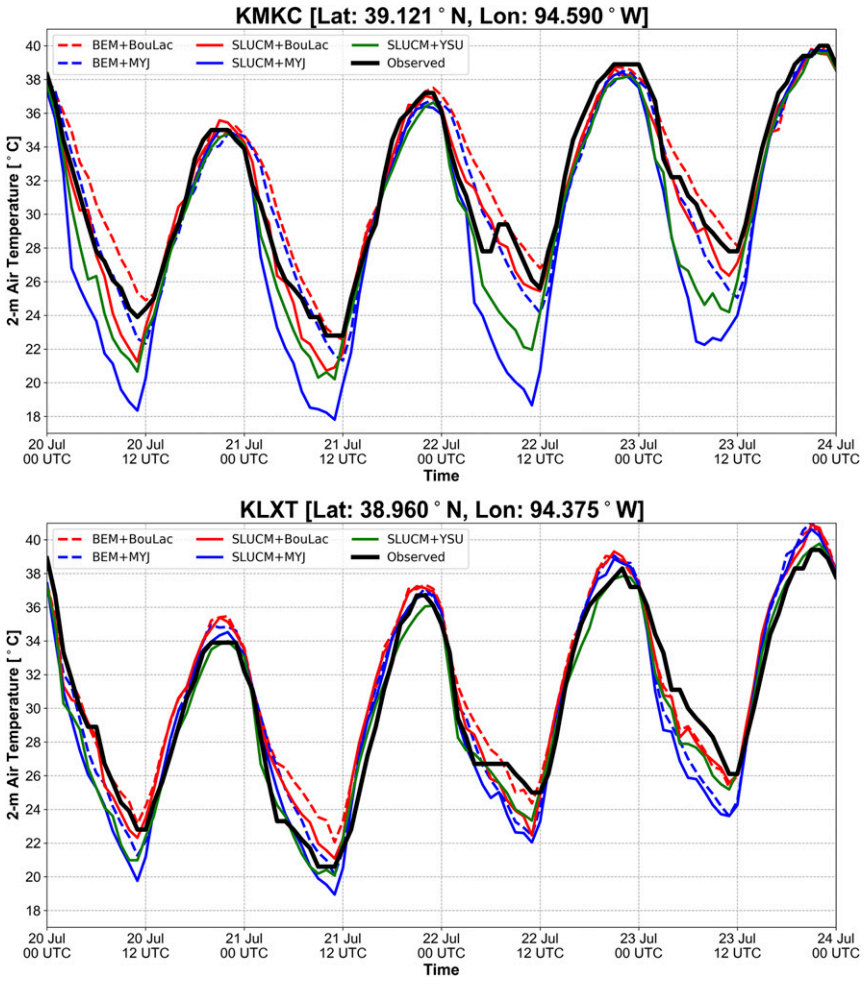

FIG. 2. Hourly modeled T_{2m} (°C) for each UCM + PBL configuration (colored, with key inset) compared with observed values (black) for the period between 0000 UTC 20 Jul and 0000 UTC 21 Jul 2012 at (top) KMKC and (bottom) KLXT.

and air conditioning usage. Because BEP + BEM is relatively similar in structure to BEP alone, only the coupled system is used in sensitivity tests along with SLUCM to assess and validate the performance of WRF.

Three boundary layer parameterizations are also assessed: the Mellor–Yamada–Janjić (MYJ) scheme (Janjić 1994), the Bougeault–Lacarrere (BouLac) scheme (Bougeault and Lacarrere 1989), and the Yonsei University (YSU) scheme (Hong et al. 2006). These schemes are important since they represent mixing in the lower atmosphere, which can greatly alter surface temperatures.

Simulations are performed for each possible combination of UCM and PBL scheme to examine its ability to replicate the diurnal cycle of 2-m temperature T_{2m}. The YSU scheme is only paired with SLUCM since it is incompatible with BEP+BEM, resulting in a total of five runs. Simulations are initialized at 1200 UTC 19 July 2012 and continued through 0000 UTC 24 July, which is during a period of elevated temperatures. The first 12 h of model output is removed to avoid issues with model spinup.

Simulated T_{2m} is compared with hourly measured values obtained from National Weather Service Automated Surface Observing System (ASOS) stations at the Kansas City Downtown Airport (KMKC) in the core of the UHI, and at Lee's Summit Municipal Airport (KLXT) outside of the city (Fig. 2). The mean bias estimate (MBE), root-mean-square error (RMSE), and Pearson correlation coefficient (PCC) are calculated at both ASOS locations over all hours, and also for just daytime (1300–0100 UTC) and nighttime (0200–1200 UTC) periods to examine WRF's ability to capture both the elevated high and low temperatures associated with UHIs, each of which are critical factors contributing to heat-related illness and mortality in urban areas (Murage et al. 2017).

A summary of the validation metrics computed for both chosen locations and across the three time periods is presented in Table 1. SLUCM + MYJ and SLUCM + YSU produces substantial nocturnal cold biases in the overnight hours, particularly in the urban setting of KMKC. The observed biases demonstrate that these configurations are inadequate for running simulations of the different greening scenarios. The

TABLE 1. Validation metrics (MBE, RMSE, and PCC) computed using modeled and observed ΔT_{2m} (°C) at the KMKC and KLXT ASOS stations for all WRF sensitivity runs. Calculations are performed over all times, daytime periods (1300–0100 UTC), and nighttime periods (0200–1200 UTC).

	All			Day			Night		
Configuration	RMSE	MBE	PCC	RMSE	MBE	PCC	RMSE	MBE	PCC
					KMKC				
BEM + BouLac	1.48	0.61	0.96	0.89	−0.22	0.98	1.97	1.62	0.95
BEM + MYJ	1.37	−0.45	0.97	1.18	−0.68	0.98	1.56	−0.18	0.92
SLUCM + BouLac	1.12	−0.54	0.98	0.75	−0.33	0.99	1.45	−0.78	0.96
SLUCM + MYJ	3.68	−2.77	0.96	1.27	−0.94	0.98	5.28	−4.96	0.90
SLUCM + YSU	2.28	−1.75	0.97	0.98	−0.81	0.99	3.22	−2.89	0.91
					KLXT				
BEM + BouLac	1.52	0.85	0.97	1.42	1.11	0.98	1.64	0.54	0.91
BEM + MYJ	1.59	−0.04	0.96	1.16	0.75	0.98	1.99	−1.00	0.87
SLUCM + BouLac	1.40	0.43	0.97	1.39	1.03	0.98	1.43	−0.29	0.92
SLUCM + MYJ	1.87	−0.64	0.96	1.04	0.53	0.98	2.54	−2.05	0.90
SLUCM + YSU	1.31	−0.64	0.98	0.82	−0.08	0.98	1.72	−1.32	0.95

BEP + BouLac simulation produces a consistent warm bias during the nighttime period at KMKC. Agreement between modeled and observed T_{2m} is better in the remaining two simulations, with RMSE values at both locations and all time periods falling within 2°C. SLUCM + BouLac slightly outperforms BEP + MYJ by most metrics. Given the relatively strong performance of SLUCM + BouLac, the significantly less computational expense of SLUCM, and widespread use of SLUCM in current research, SLUCM + BouLac is selected to use in the experimental runs. All WRF options in the subsequent analysis are the same and listed Table 2.

3. Control and experimental simulations setup

Three persistent periods of high summertime temperatures with stagnant synoptic conditions are examined. Each case spans a total of five days, beginning and ending at 0000 UTC: 16–21 July 2011, 19–24 July 2012, and 24–30 August 2013. While the region has been impacted by other intense periods of heat, the selected cases are chosen due to their proximity to the publication of the geographic data used in the model system (2011), the 2010 census data, lack of cloud cover and precipitation, and the availability of NAM analysis data used to initialize WRF simulations.

WRF is run four times for each of the three cases. The control simulation has no modifications to the input geographic datasets. For the experimental simulations, the vacancy rate within the focus area of 28% is used to define three greening scenarios of varying intensity: 1) a ''conservative'' strategy in which one-half of available vacant space is converted to green space (14%), 2) a ''moderate'' strategy in which all available vacant space is converted (28%), and 3) an ''aggressive'' strategy that accounts for the conversion of all available vacant land plus the greening of occupied spaces with features such as street trees, vegetation, and green boulevards (42%). The first 12 h of output are discarded from all analyses to avoid the model spinup period.

Input geographic datasets are modified to represent the corresponding greening within this area. Fractional LANDUSEF values for the NLCD urban categories are reduced by 14%, 28%, and 42% for the conservative, moderate, and aggressive greening strategies, respectively, and are replaced by NLCD category 14 (cropland/natural vegetation mosaic) to reflect the conversion of the abandoned area to diverse green spaces in the urban environment. Land-use categories are subsequently recalculated, and the value of LU_INDEX at each point is updated.

Values for FRC_URB2D and IMPERV within the area are proportionally reduced by the sum of all reduced urban fractional values to account for the loss of impervious surfaces due to greening, while CANFRA values are proportionally increased to represent the expansion of the tree canopy. A summary of mean values for relevant geographic input parameters within the focus area during the control run and each greening strategy is presented in Table 3.

TABLE 2. List of parameterization schemes used to configure WRF.

Physics option	Parameterization	Reference
Microphysics	WRF single-moment 3-class	Hong et al. (2004)
Shortwave radiation	RRTMG	Iacono et al. (2008)
Longwave radiation	RRTMG	Iacono et al. (2008)
Surface layer	Eta similarity scheme	Janjić (1994)
Cumulus (d01 only)	Kain–Fritsch scheme	Kain (2004)
Boundary layer	Bougeault–Lacarrere scheme	Bougeault and Lacarrere (1989)
Land surface	Unified Noah LSM	Tewari et al. (2004)
Urban physics	Single-layer urban canopy model	Chen et al. (2011)

TABLE 3. Mean values for input WRF geographic parameters for control simulations (CTL) and simulations reflecting the conservative (CON), moderate (MOD), and aggressive (AGR) greening strategies.

Input parameter	CTL	CON	MOD	AGR
LANDUSEF, developed low intensity	0.42	0.36	0.30	0.24
LANDUSEF, developed medium intensity	0.39	0.33	0.28	0.23
LANDUSEF, developed high intensity	0.10	0.08	0.07	0.06
LANDUSEF, cropland/natural vegetation mosaic	0.00	0.06	0.12	0.18
FRC_URB2D	0.64	0.58	0.52	0.46
IMPERV	0.47	0.33	0.19	0.09
CANFRA	0.12	0.19	0.26	0.33

Although modifications made to the urban landscape in the three greening scenarios are not sweeping, they do represent levels of greening that could be realistically adopted in the focus area while also preserving the form and functionality of its neighborhoods. Furthermore, given the significant time and capital investments required to implement greening strategies on a large spatial scale, the strategies presented here offer a more practical outlook on potential UHI mitigation than other past studies of this manner (e.g., Zhou and Shepherd 2010; Morini et al. 2016; Fu and Weng 2017). While other social and political intricacies of urban greening are beyond the scope of this study, it is nonetheless anticipated that the results of these simulations can be interpreted as a baseline for the potential temperature impact, if any, of these greening strategies.

4. Results

a. Baseline characteristics

Mean T_{2m} from the control simulation of case 1 (16–21 July 2012) are given for the daytime (1300–0100 UTC, 0800–2100 LST) and nighttime (0200–1200 UTC, 2100–0800 LST) periods in Fig. 3. Warmer air temperatures are present in the Kansas City urban core, while mean T_{2m} in the more forested suburban areas surrounding it are generally lower. Although local cooling is the most direct effect of land-use conversion, Oliveira et al. (2011) and Declet-Barreto et al. (2013) have also demonstrated the benefits of downwind advective cooling in areas surrounding of urban green spaces. During the summer, the wind is most typically from the south, suggesting that cooler air associated with implemented green spaces is likely to be transported toward the residential area north of the focus region, which exhibits a similar pattern of high vacancy rates.

To investigate the diurnal evolution of the UHI in the control simulations, hourly UHI intensity is analyzed (Fig. 4). The UHI intensity is calculated as the simple difference in simulated T_{2m} between the KMKC (urban) and KLXT (nonurban) ASOS locations. The simulated UHI exhibits a clear periodicity across all three control cases, peaking in intensity at approximately 0300 UTC (2200 LST) and reaching a minimum at approximately 1400 UTC (0900 LST). Mean UHI intensity for

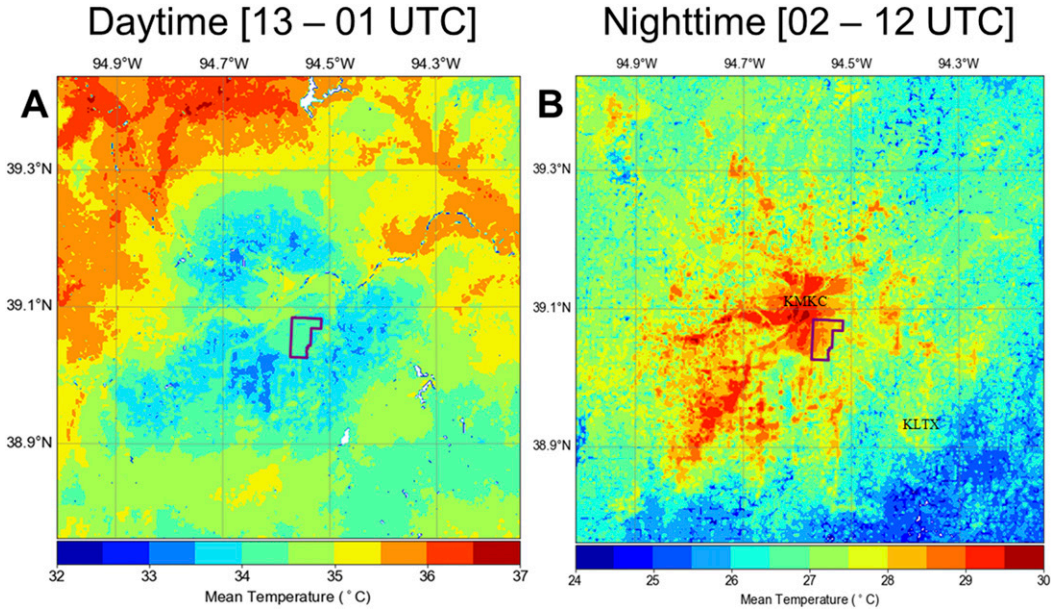

FIG. 3. Mean T_{2m} (°C; shaded) in d03 over the (a) daytime period (1300–0100 UTC) and (b) nighttime period (0200–1200 UTC) between 16 and 21 Jul 2012 (case 1), with the focus area highlighted (purple outline).

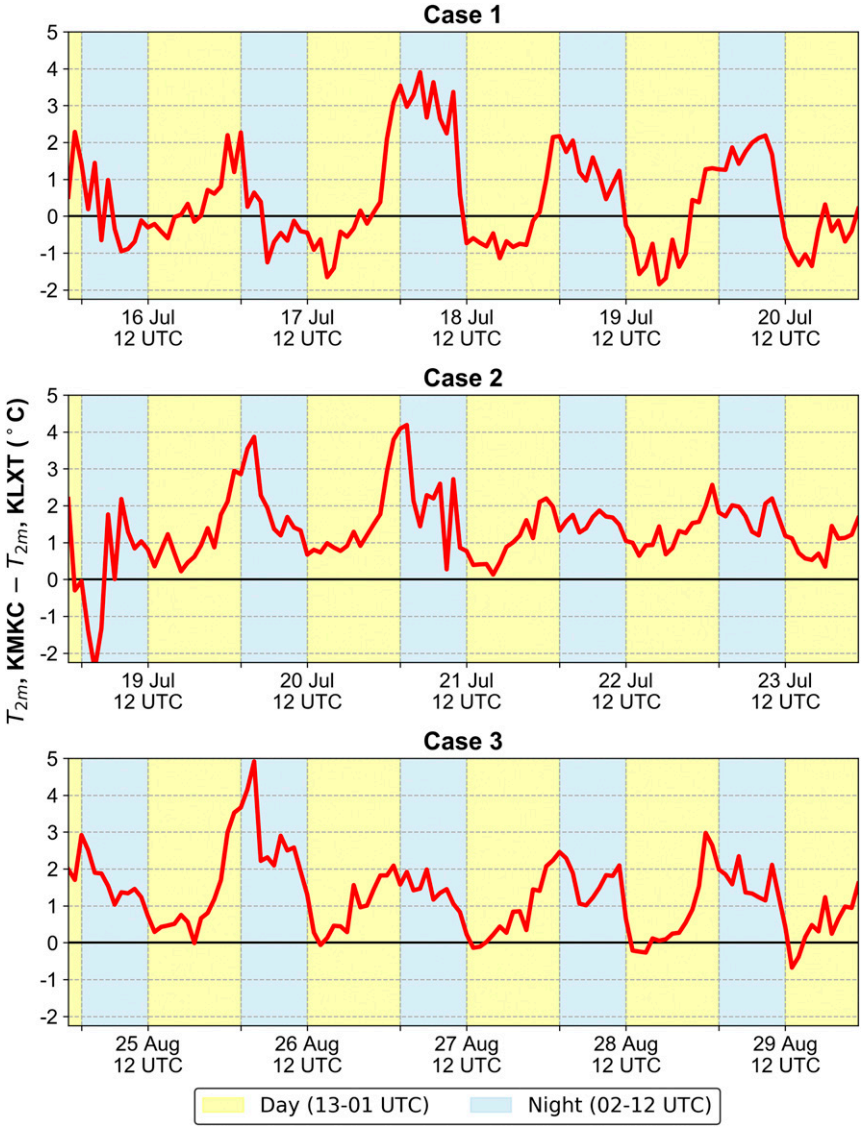

FIG. 4. Hourly modeled UHI intensity (°C) for each case study, calculated as the difference in simulated T_{2m} at KMKC and KLXT. Daytime and nighttime periods are highlighted in yellow and blue, respectively.

all simulations is 1.4°C during the day and 0.6°C overnight, although maximum nighttime values reach upward of 4°C. The UHI intensity is occasionally negative, most notably during the daytime periods of case 1. This so-called urban cool island has been observed to occur during the day in other locations, is usually fairly weak, and is attributed to factors such as higher thermal inertia in urban areas as compared with rural areas (Bohnenstengel et al. 2011). The Kansas City UHI resolved by the control simulations is consistent in structure and diurnal variation with numerous previous observational studies at other locations, such as Tran et al. (2006), Azevedo et al. (2016), and Tan et al. (2010).

Daytime and nighttime mean temperature distributions across the region's diverse LULC are binned by each grid point's dominant NLCD land-use classification to highlight the local influence of LULC (Fig. 5). For all cases at night, the distributions of T_{2m} in grid cells where urban land use is dominant (NLCD categories 23–26) expectedly and consistently show an increase in both mean and median T_{2m} with increased urban density. Urban-classified cells show little to no UHI signal during the daytime period when compared with forested, grassland, or agricultural areas, which is attributed to the cool-island effect.

Overnight, greater mean, median, and quartile T_{2m} are observed for urban-dominant cells when compared to other categories. The range of values over urban cells tends to be wider than those during the day periods for several reasons. Location plays a large role in that an urban grid cell surrounded by

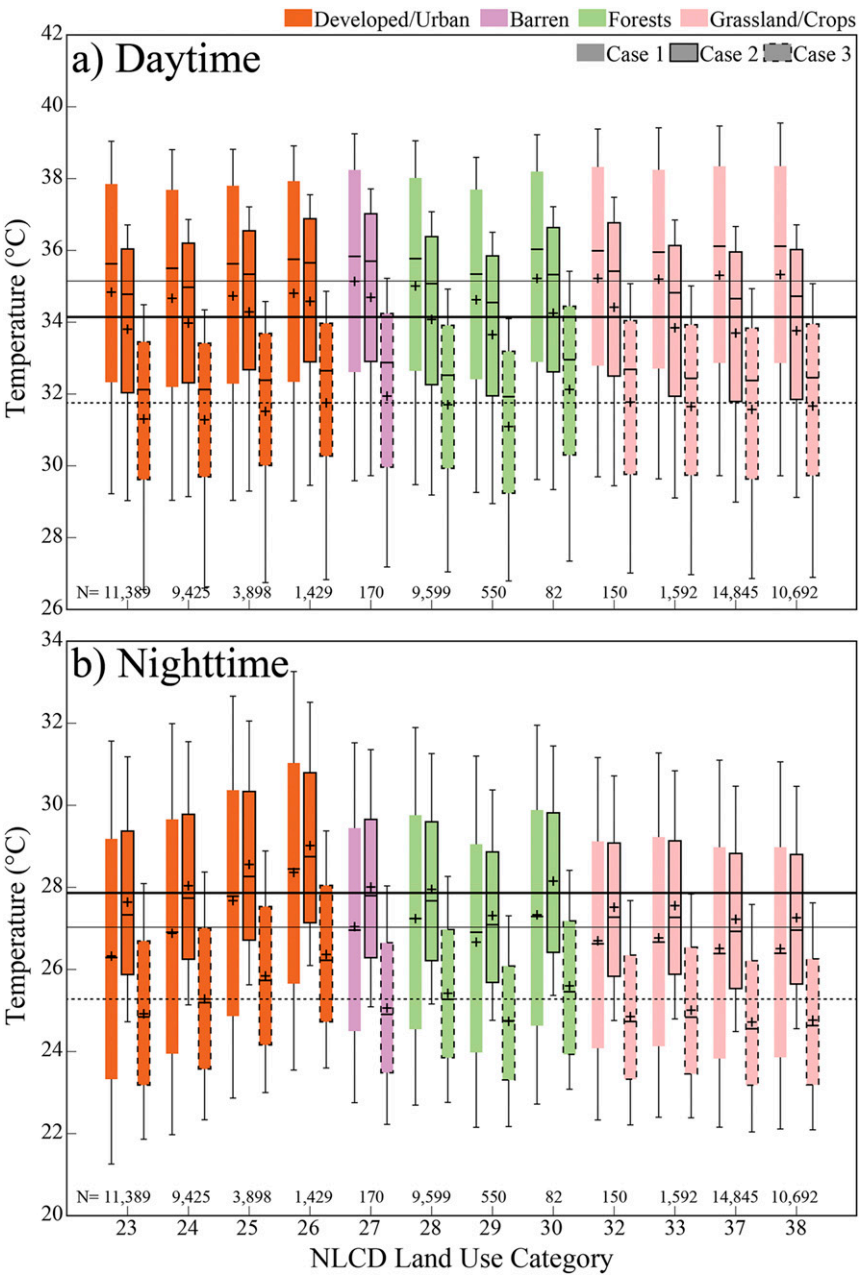

FIG. 5. The (a) daytime and (b) nighttime T_{2m} (°C) grouped by NLCD land-use category for the control simulations of case 1 (no border), case 2 (solid border), and case 3 (dashed border). Boxes extend to the 25th and 75th percentiles, whiskers extend to the 10th and 90th percentiles, the horizontal line is the median, and the plus sign is the mean. The number of grid points in d03 for each category is indicated at the bottom of each panel. Horizontal lines indicate the mean for case 1 (thin), case 2 (thick), and case 3 (dashed).

nonurban LULC will show much different temperatures than an urban cell surrounded by other urban cells, such as downtown. Given that the model system uses fractional land-use values to calculate T_{2m} instead of just the dominate category, some of this variability may be due to the presence of less-dominant LULC types in grid cells within a dominant urban LULC. Another factor in nighttime temperature variability is the formation of the stable nocturnal boundary layer, which coincides with a reduction in turbulent mixing and vertical heat and momentum transport and can feed back onto surface cooling rates and thus result in the local air temperatures having a greater sensitivity to surrounding land-cover characteristics.

Results from Figs. 4 and 5 also highlight that since the UHI intensity is greatest overnight, then the implemented green

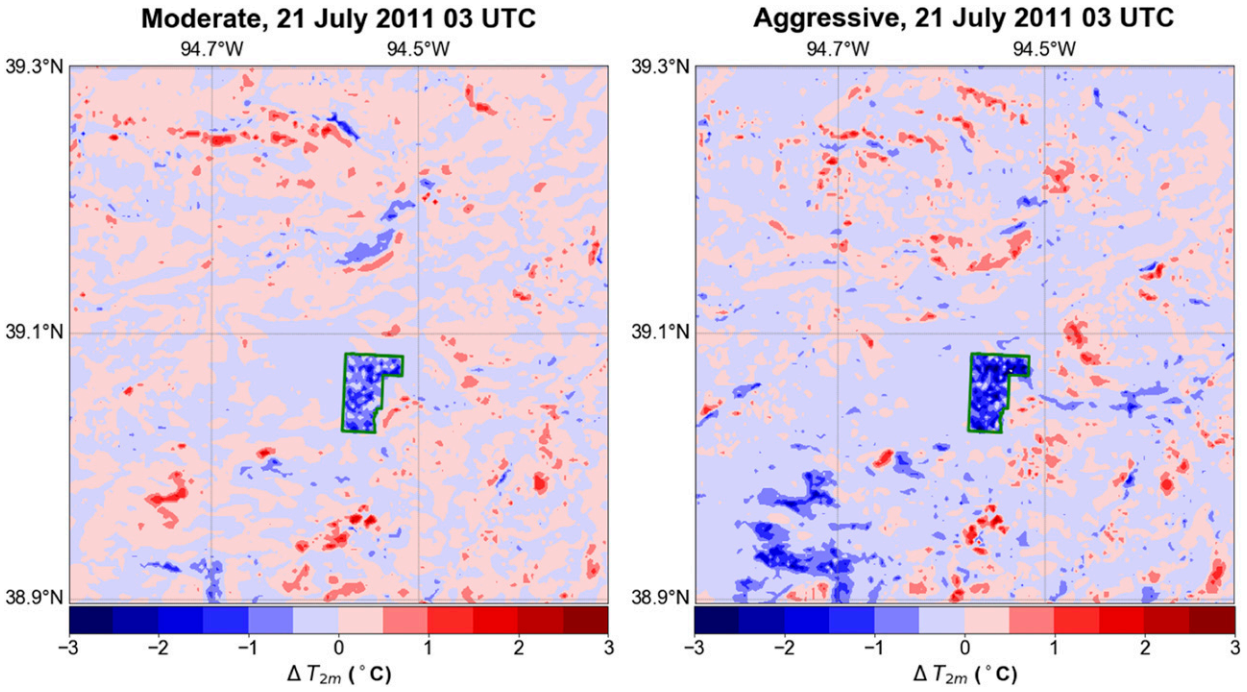

FIG. 6. The ΔT_{2m} values (shaded; °C) at 0300 UTC 21 Jul 2011 for the (left) moderate and (right) aggressive greening strategies. The focus area is denoted with a green outline.

spaces would have a greater impact on reducing overnight lows than daytime highs. Although this may not serve as a significant means of mitigating the extreme *daytime* high temperatures associated with an array of public health concerns, a cooler temperature *overnight* has been identified as a critical factor in reducing heat-related illnesses and morbidity in urban areas (e.g., Frumkin 2002; Murage et al. 2017).

Overall, the control simulations demonstrate WRF's ability to reproduce the UHI that are consistent with observed trends in its diurnal evolution and its sensitivity to varying LULC qualities (e.g., Estoque 2017). The control runs also show the value of increasing the inner domain resolution beyond levels typically found in other UHI simulations using WRF, which will allow the experimental greening simulations to be performed and analyzed with greater confidence. Although urban greening in this study is not enacted where T_{2m} is the most enhanced by the UHI, the focus area lies within a region prone to its effects and with a high rate of vacant lots.

b. *Local impacts of urban greening*

To quantify the potential mitigation of the UHI from the prescribed conversion of current vacant lots to green spaces, the difference in 2-m air temperature (ΔT_{2m}) between each case's control simulation and the three experimental runs (experimental–control) is calculated. As an example, Fig. 6 depicts ΔT_{2m} after sunset (0300 UTC 21 July 2011). Small-scale differences between the experimental and control runs are prevalent throughout the domain and are associated with the turbulent nature of the lower atmosphere but behave as white noise. Despite the noisy background at single times, there is a clear cooling signal within the focus area. This exemplifies the local cooling effect that is observable to varying degrees across all cases and greening magnitudes.

To assess the projected local impacts of urban greening within just the focus area where the greening is enforced, ΔT_{2m} of all grid points within the focus area by hour for each case and greening strategy is summarized in Fig. 7. Although the impact of the greening is not necessarily evenly distributed throughout the focus area, this offers a simple and direct assessment of the potential utility of greening as an avenue to potential UHI mitigation. The greening impacts usually increase downwind, and nonlocal effects will be explored later.

Although the impacts of simulated urban greening exhibits variation across cases and over the diurnal cycle, the modifications made to land cover within the focus area in the model system nonetheless result in a general reduction of local T_{2m} as expected. The cooling associated with these modifications is most apparent from approximately 0400–1500 UTC (2300–1000 LST) across all cases, encompassing the majority of the overnight and early morning period where atmospheric UHI intensity has been observed to be greatest (e.g., Voogt 2007; Azevedo et al. 2016). For case 1, cooler T_{2m} values persist further into the daytime period, with median cooling values greater than 0.70°C through 2200 UTC in the aggressive greening scenario. The effects of land-use conversion are generally smaller during the daytime period. This is attributable to increased vertical mixing within the daytime boundary layer.

The magnitude of local nocturnal cooling in the conservative greening simulations is minimal, as mean and median ΔT_{2m} values rarely exceed −0.25°C and positive ΔT_{2m} values are

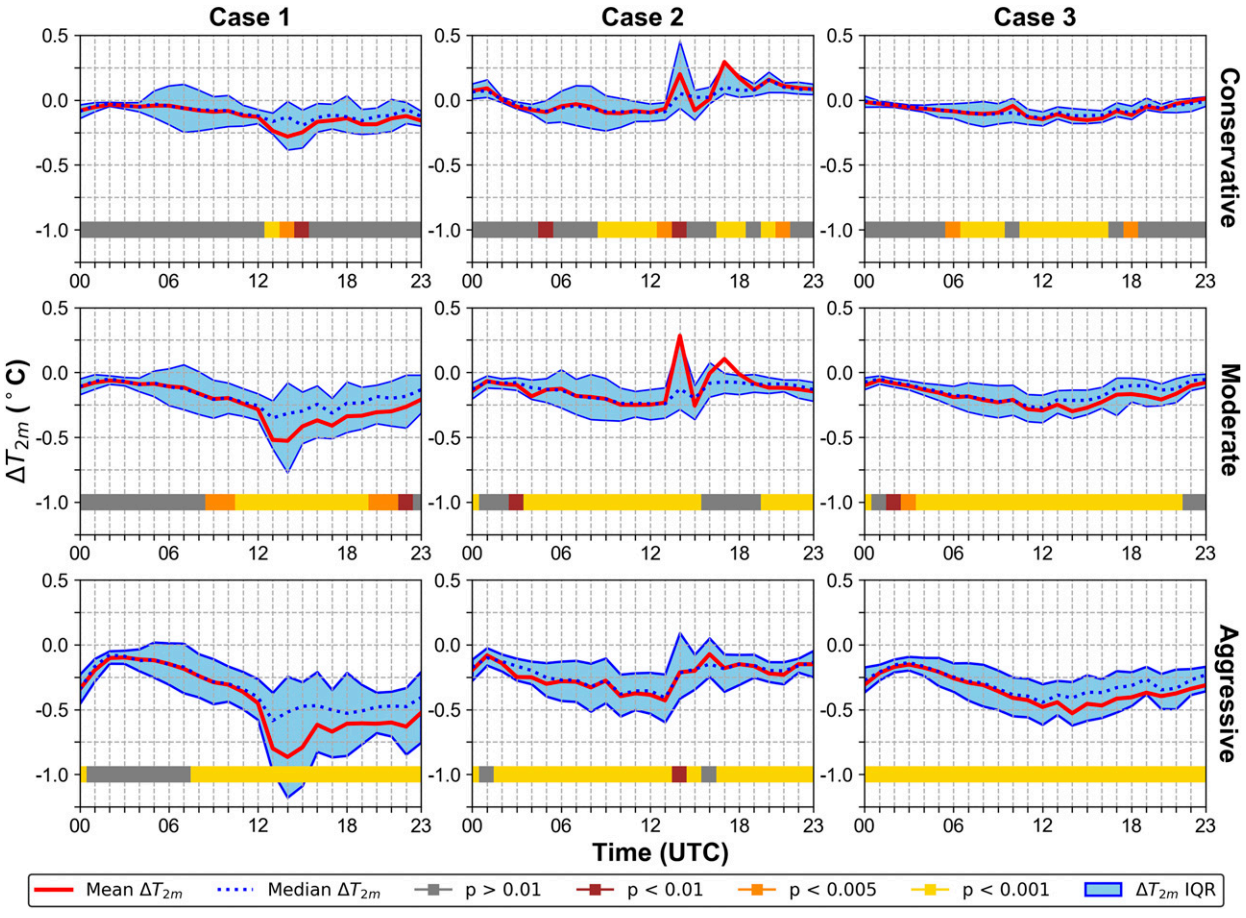

FIG. 7. The ΔT_{2m} (°C) within the focus area for each case (columns) and strategy (rows), consisting of ΔT_{2m} values at all grid points inside the focus area, binned by hour (UTC), and showing the mean (solid red), median (dashed blue), and interquartile range (blue shaded). Statistical significance of the simulated cooling is denoted in the band below each panel at the $p < 0.01$ (brown), $p < 0.005$ (orange), and $p < 0.001$ (yellow) levels.

often captured within the interquartile range of the distribution. Simulations carried out using moderate and aggressive greening strategies produce a more noticeable nocturnal cooling signal. Mean and median hourly ΔT_{2m} values during the overnight period generally surpass −0.25°C for moderate greening simulations and −0.50°C for aggressive greening simulations. Furthermore, the interquartile range of the moderate and aggressive ΔT_{2m} distributions rarely capture any positive values during the overnight hours.

The cooler temperatures of the greening scenarios is associated with a change in the partition between sensible heat (SH) and latent heat (LH) at the surface that is driven by an increase of evapotranspiration from more vegetation and a reduction of SH related to the decrease of urban surfaces as well as a decrease of sources that contribute to anthropogenic heating. To illustrate these changes in more detail, the evaporative fraction (EF) is used to quantify the partition between LH and SH:

$$\mathrm{EF} = \frac{\mathrm{LH}}{\mathrm{LH} + \mathrm{SH}}.$$

The average daytime EF is depicted in Fig. 8 and demonstrates the impact to the surface energy partition under the three greening strategies for each case. Beginning with the control simulations, the EF in case 1 and 2 is similar, but case 3 has a higher EF. The higher EF in case 3 is attributed to greater precipitation prior to this time period that resulted in greater soil moisture at the time of model initialization. The response of EF to greening for the conservative scenario is an increase of about 0.05 from the control runs. The difference of EF from the control run increases to 0.10 and 0.15 for the moderate and aggressive scenarios, respectively. Given the greater amount of moisture in case 3, a slightly larger increase in the EF is seen as the amount of greening increases. In general, the response to greening for these cases follows a consistent pattern for all three cases. It should be noted that these three cases are for cloud-free conditions, and more nonlinear interaction may occur if cloud feedbacks are present.

To more rigorously quantify whether the potential cooling effects of urban greening within the model system were in fact meaningful, a two-sample Student's t test is performed between the control and experimental simulations at each hour

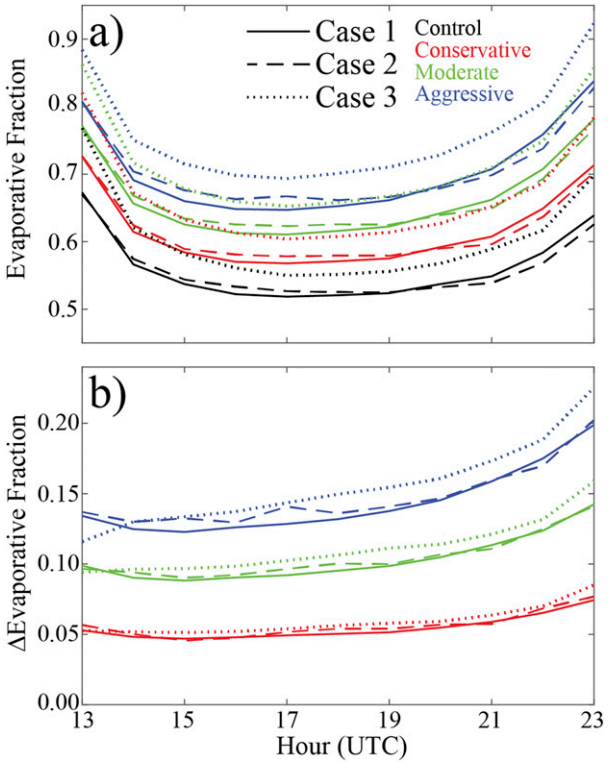

FIG. 8. (a) The average daytime evaporative fraction within the focus area for case 1 (solid), case 2 (dashed), and case 3 (dotted) for each simulation: control (black), conservative (red), moderate (green), and aggressive (blue). (b) Difference of evaporative fraction between the three different greening scenarios and the control simulation.

and for each case and greening strategy to determine if the difference is significantly different than zero. The p values from these tests are included in Fig. 7. The cooling signals produced by the conservative simulations display few instances of statistical significance compared to the more aggressive scenarios. The moderate and aggressive greening scenarios tend to produce greater cooling that was significant at or below the $p = 0.001$ level. Within the moderate simulations, this level of significance was confined mostly to the overnight through early afternoon period, ranging from approximately 0400 to 2000 UTC across each of the three cases. Conversely, for the aggressive greening simulations, this period extended throughout the majority of the diurnal cycle.

The results obtained from the significance tests here are by no means unexpected. They do however further support the idea that countering the warming within the UHI via land-use conversion appears to only be effective in more extensive greening scenarios, which may require a more substantial investment that requires the use of significant social, financial, and political capital. Since conversion of green space is constrained by limiting the changes to *existing* abandoned properties, this provides insight into the merits of a more feasible strategy. Atmospheric temperatures can really only be reduced by the more aggressive strategies.

c. *Nonlocal impacts of urban greening*

While converting to green space provides local cooling effects, observational studies such as Oliveira et al. (2011) and Chow et al. (2011) demonstrate that the cooling is not necessarily confined to just the converted spaces. As discussed in Doick et al. (2014), advective processes often result in an expansion of the park cool island in urban areas to surrounding nonvegetated areas. Like the observed diurnal cycle of cooling intensity within green spaces, the nonlocal effects of greening are also strongest during the nighttime. Given that these additional benefits of green space implementation may further justify the pursuit of UHI abatement through land-use conversion, it is important to examine the strength and extent of simulated downwind cooling surrounding the focus area for this study.

The synoptic flow over Kansas City is generally from the south in the summer months, so the north side is typically the downwind side. Furthermore, the block-level census shows locations north of the focus area have similarly high residential vacancy rates. Given that these areas are located where cold air advection from the park cool island would be climatologically most frequent, the overarching UHI mitigation goals could possibly extend beyond just the local areas with implemented green spaces. As a result, ΔT_{2m} is assessed across each case and greening scenario for model grid locations downwind from the boundaries of the focus area at each time step.

To determine the cooling in grid cells downwind of the focus area, it is necessary to determine which cells would be considered downwind from the greening area boundaries at each time step. To do so, the simulated wind direction is used to determine the downwind edge of the focus area, then the bounds of the downwind area are placed at the ends of this edge and extended outward 10 km in the direction of the wind. An example of this process is given in Fig. 9 showing ΔT_{2m} at 0000 UTC 30 August 2013 for the aggressive greening strategy. Once the downwind grid points are determined, the distance between each point and the upwind edge of the focus area are calculated.

Obtaining a good metric to represent the downwind cooling is not trivial. For each time step, all ΔT_{2m} within 0.2-km distance bands are used to find a maximum and mean ΔT_{2m}. The maximum ΔT_{2m} represents an upper-bound on the downwind cooling, which can be influenced by outliers or spurious data. The median and mean ΔT_{2m} represent more conservative metrics. The mean can be influenced by outliers as well, and both the mean and median can be significantly influenced by the definition of the downwind area. For example, the mean and median will show greater cooling if the downwind box does not extend all the way out to the edges but only extends halfway to the edges. By displaying both the conservative and upper-bound methods, it should provide a better sense of the downwind impacts.

There is clearly a cooling downwind of the greened area in Fig. 9 that tends to diminish about 6 km downwind of the focus area. The median and mean indicate cooler temperatures that slowly diminish from 3 to 6 km and are fairly close for this and other times, so subsequent analysis will only consider the median. The maximum tends to follow the same trend with values about double that of the median.

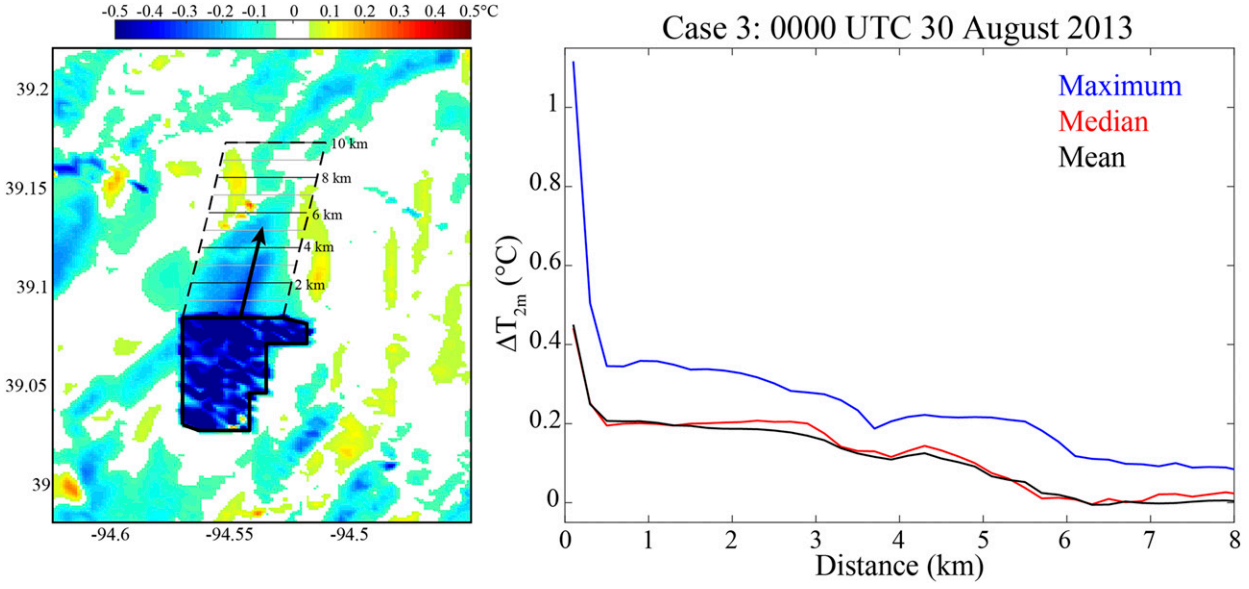

FIG. 9. Example of obtaining anomalies downwind of the focus area at 0000 UTC 30 Aug 2013: (left) ΔT_{2m} (°C) with the focus area outlined in black, the downwind area polygon outlined with the dashed black line, the thin lines indicating distance from the focus area, and an arrow representing the wind direction, and (right) the maximum, median, and mean cooling within each distance band.

To summarize the downwind effect, the maximum and median downwind cooling from individual times as shown in Fig. 9 are grouped by time of day and greening strategy. Then, the median and interquartile range of those are found (Fig. 10). There is no difference in downwind cooling in the conservative case since the mean and its interquartile range is clearly centered on zero. The maximum difference is only attributed to noise. The time of day also plays a large role in the downwind cooling such that even in the aggressive cases the early and late day time periods show a minimal impact. This can be attributed to the deep, well-mixed boundary layer during the day. The advection of cooler air from the focus area to downwind areas does tend to produce a weak but noticeably cooler ΔT_{2m}, mostly confined to locations immediately next to the focus area boundary.

The influence of the downwind cooling becomes largest overnight and into the morning with a marked cooling extending well past the focus area for the aggressive greening strategies. At most, maximum values tend to be 0.5°C just downwind of the edge, which is slightly less than values found in Fig. 7. The difference decreases rapidly over the first 500 m, and then decreases more slowly farther downwind. The overnight time period aligns with the peak of the local cooling effects, making the stronger advection seen here unsurprising due to the stronger local temperature gradient present across the area.

Downwind reductions of ΔT_{2m} associated with the conservative greening strategy are negligible, the moderate strategy is weak at best, but the aggressive strategy does have more substantial impacts downwind, albeit with modest magnitudes. In terms of similar studies regarding the extension of the park cool island into surrounding areas, both the extent and magnitude of downwind cooling observed in these simulations is in line previous observational studies such as Doick et al. (2014) and Feyisa et al. (2014) as well as modeling studies such as Declet-Barreto et al. (2013).

5. Summary

Elevated near-surface air temperatures pose an increasing threat to residents of the world's cities with impacts expected to increase in the coming decades due to the combined forces of urbanization and anthropogenic global warming (Revi et al. 2014; IPCC 2014; Frumkin 2002). Recent efforts have been made to counteract the UHI by implementing green spaces into urbanized areas to reduce the air temperature (Schilling and Logan 2008; Hart and Sailor 2009; Oliveira et al. 2011). While the potential impact of urban greening can be difficult to anticipate, the use of numerical weather simulations to analyze the thermal impacts of land-use conversion offers a useful avenue to assess green space implementation scenarios (Santamouris 2013; Papangelis et al. 2012; Zhou and Shepherd 2010). In accordance with recent urban greening efforts (e.g., Colasanti et al. 2012; Meerow and Newell 2017), a portion of the Kansas City area with high vacancy rates is identified as a potential location where large-scale green space implementation would be potentially feasible (Fig. 1b). By using atmospheric modeling and a realistic greening strategy of converting abandoned properties in economically underserved portions of the Kansas City metropolitan area, we explore the potential cooling impact.

After performing a series of sensitivity tests, the best performing model configuration was found and used as the baseline. The control run indicated that the UHI intensity reaches up to 5°C during the overnight hours (Fig. 4). Three potential urban greening scenarios of increasing extent (conservative, moderate, and aggressive) are used in the experimental simulations based on local residential vacancy rates within the focus

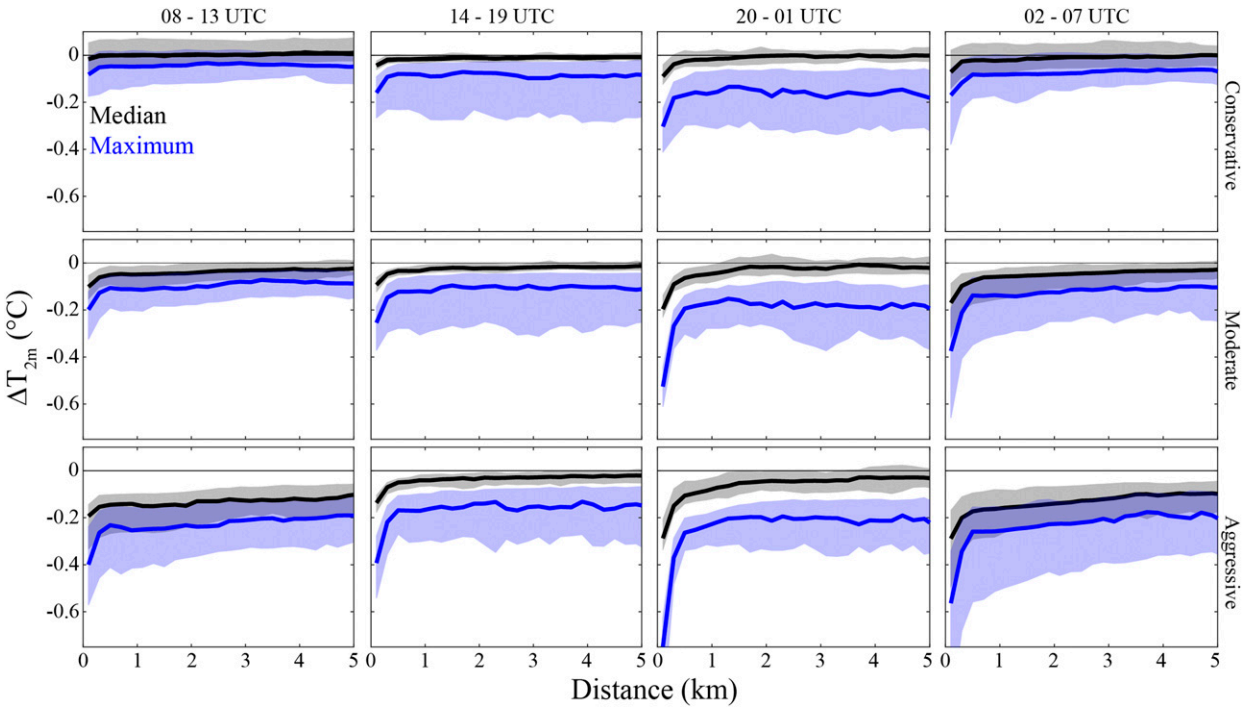

FIG. 10. The median (solid lines) and interquartile range (shaded regions) of the maximum (blue) and median (black) downwind ΔT_{2m} (°C) by distance band for all cases grouped by time of day and greening strategy.

area, and the high-resolution LULC data within the model system are modified to reflect these potential scenarios. The WRF runs encompass three 5-day periods of elevated summertime heat for the control run with no LULC modifications and the three greening scenarios.

Given the complex nature of surface–atmosphere processes over urban areas, there are several limitations that need to be clearly stated. One of the criteria for selecting the three cases included selecting periods with relatively low cloud cover to minimize uncertainty associated with the model's ability to correctly represent cloud fields and to avoid feedbacks with cloud cover that would add an additional layer of complexity. A change of the land use over a city will influence factors such as the temperature, humidity, aerosol concentration, amount of anthropogenic heat, and the near-surface divergence field due to a change of surface roughness. All of these factors affect both cloud cover and precipitation (e.g., Shepherd 2005; Niyogi et al. 2020) and are sensitive to model configuration, including the cumulus parameterization and microphysics. Given the clear skies typical during the three cases presented here, the model sensitivity to these parameters is not a major factor. For this reason, we could use relatively simple parameterization schemes such as Kain–Fritsch for the cumulus parameterization and the WRF single-moment 3-class microphysics scheme. However, when conditions are not clear the importance of the model parameterizations becomes much more important. The results shown here show the responses under clear conditions.

Another aspect is that this work is focused on one region of one particular city to address issues important to the local area. Since each city has different morphologies, building compositions, and amounts of anthropogenic heating, the changes to the landscape within different types of cities may have different responses. For example, Niyogi et al. (2020) linked the amount of anthropogenic heating used in WRF to changes in the cloud and rainfall, and Yang et al. (2016) explored the changes to the heat island intensity of Beijing, China, using a compact and dispersed form of the city. Incorporation of more green space in a more compact or more dispersed city will have different impacts. However, an advantage of our approach is that it considers a more targeted approach by using information on current vacant lots.

To examine the cooling impact of the implemented green spaces in each experimental simulation, the ΔT_{2m} is calculated as the difference in T_{2m} between the experimental and control simulation (Fig. 7). Overall, the conservative greening simulations show minimal UHI abatement within the focus area. Results from the moderate and aggressive greening scenarios indicate that more extensive urban green space implementation has the potential to reduce median nocturnal temperatures within the focus area by 0.5° to 1.0°C, particularly overnight.

Given the park cool island that can extend this cooling downwind via cold air advection, the potential for downwind cooling is also explored. These results indicate that the conservative greening strategy has no downwind impact, the moderate strategy shows only modest impacts, but the aggressive strategy did show greater cooling downwind, however the cooling is not large.

Similar experiments are conducted in studies such as Zhou and Shepherd (2010), Papangelis et al. (2012), Morini et al. (2016), and Fu and Weng (2017). While past work uses numerical

simulations to examine UHI abatement, these depictions of urban greening have generally been sweeping changes instead of more feasible scenarios (e.g., converting to all green roofs across an entire city). Here, we present simulations of urban greening that are both more feasible and targeted within a region that might benefit from other aspects of green space implementation. Because of the more feasible nature in which urban greening has been implemented in this study, both the local and downwind effects of greening indicated that significant cooling is confined to the moderate and aggressive strategies and the majority of significant cooling impacts have a magnitude at or below 1.0°C.

Although only three case studies at a single location under similar synoptic weather patterns are considered, the results are not likely to be much different under other conditions. While the reduction of T_{2m} by 0.5°–1.0°C is unlikely to eliminate heat-related illnesses or mortality during summertime heat waves, these results present more realistic numbers for consideration when exploring potential avenues for UHI mitigation. Of course, the large-scale conversion of vacant land at a level reflecting the moderate or aggressive greening strategies of this study still requires significant financial and political capital. However, the potential benefits of both reducing the UHI and also driving reinvestment in a community's natural environment make it a useful option to explore in areas with high land-use conversion potential such as the focus area of this study. UHI mitigation might be a secondary reason for land-use conversion, but it may at least provide an additional incentive.

Acknowledgments. We thank the reviewers for their constructive comments.

REFERENCES

Akbari, H., and Coauthors, 2016: Local climate change and urban heat island mitigation techniques—The state of the art. *J. Civ. Eng. Manage.*, **22**, 1–16, https://doi.org/10.3846/13923730.2015.1111934.

Arnfield, A. J., 2003: Two decades of urban climate research: A review of turbulence, exchanges of energy and water, and the urban heat island. *Int. J. Climatol.*, **23**, 1–26, https://doi.org/10.1002/JOC.859.

Azevedo, J. A., L. Chapman, and C. L. Muller, 2016: Quantifying the daytime and night-time urban heat island in Birmingham, UK: A comparison of satellite derived land surface temperature and high resolution air temperature observations. *Remote Sens.*, **8**, 153, https://doi.org/10.3390/RS8020153.

Bohnenstengel, S., S. Evans, P. A. Clark, and S. Belcher, 2011: Simulations of the London urban heat island. *Quart. J. Roy. Meteor. Soc.*, **137**, 1625–1640, https://doi.org/10.1002/QJ.855.

Boswell, M., A. Greve, and T. Seale, 2019: *Climate Action Planning: A Guide to Creating Low-Carbon, Resilient Communities*. Island Press, 380 pp.

Bougeault, P., and P. Lacarrere, 1989: Parameterization of orography-induced turbulence in a mesobeta-scale model. *Mon. Wea. Rev.*, **117**, 1872–1890, https://doi.org/10.1175/1520-0493(1989)117<1872:POOITI>2.0.CO;2.

Chen, F., and Coauthors, 2011: The integrated WRF/urban modelling system: Development, evaluation, and applications to urban environmental problems. *Int. J. Climatol.*, **31**, 273–288, https://doi.org/10.1002/JOC.2158.

Chow, W. T., R. L. Pope, C. A. Martin, and A. J. Brazel, 2011: Observing and modeling the nocturnal park cool island of an arid city: Horizontal and vertical impacts. *Theor. Appl. Climatol.*, **103**, 197–211, https://doi.org/10.1007/S00704-010-0293-8.

City of Kansas City, Division of Community Engagement, Policy and Accountability, 2017: A segregated Kansas City is not good for our health. KCMO Public Health Connection 37, 6 pp., https://www.kcmo.gov/home/showdocument?id=3477.

Colasanti, K. J., M. W. Hamm, and C. M. Litjens, 2012: The city as an "agricultural powerhouse"? Perspectives on expanding urban agriculture from Detroit, Michigan. *Urban Geogr.*, **33**, 348–369, https://doi.org/10.2747/0272-3638.33.3.348.

Danielson, J. J., and D. B. Gesch, 2011: Global multi-resolution terrain elevation data 2010 (GMTED2010). U.S. Geological Survey Tech. Rep., 26 pp., https://doi.org/10.3133/OFR20111073.

Declet-Barreto, J., A. J. Brazel, C. A. Martin, W. T. Chow, and S. L. Harlan, 2013: Creating the park cool island in an inner-city neighborhood: Heat mitigation strategy for Phoenix, AZ. *Urban Ecosyst.*, **16**, 617–635, https://doi.org/10.1007/S11252-012-0278-8.

Doick, K. J., A. Peace, and T. R. Hutchings, 2014: The role of one large greenspace in mitigating London's nocturnal urban heat island. *Sci. Total Environ.*, **493**, 662–671, https://doi.org/10.1016/J.SCITOTENV.2014.06.048.

Estoque, R. C., Y. Murayama, and S. W. Myint, 2017: Effects of landscape composition and pattern on land surface temperature: An urban heat island study in the megacities of Southeast Asia. *Sci. Total Environ.*, **577**, 349–359, https://doi.org/10.1016/J.SCITOTENV.2016.10.195.

Feyisa, G. L., K. Dons, and H. Meilby, 2014: Efficiency of parks in mitigating urban heat island effect: An example from Addis Ababa. *Landscape Urban Plann.*, **123**, 87–95, https://doi.org/10.1016/J.LANDURBPLAN.2013.12.008.

Frumkin, H., 2002: Urban sprawl and public health. *Public Health Rep.*, **117**, 201–217, https://doi.org/10.1016/S0033-3549(04)50155-3.

Fu, P., and Q. Weng, 2017: Responses of urban heat island in Atlanta to different land-use scenarios. *Theor. Appl. Climatol.*, **133**, 123–135, https://doi.org/10.1007/s00704-017-2160-3.

Giannaros, C., A. Nenes, T. M. Giannaros, K. Kourtidis, and D. Melas, 2018: A comprehensive approach for the simulation of the urban heat island effect with the WRF/SLUCM modeling system: The case of Athens (Greece). *Atmos. Res.*, **201**, 86–101, https://doi.org/10.1016/J.ATMOSRES.2017.10.015.

Glotfelty, T., M. Tewari, K. Sampson, M. Duda, F. Chen, and J. Ching, 2013: Nudapt 44 documentation. NCAR Research Applications Laboratory Doc., 9 pp., https://ral.ucar.edu/sites/default/files/public/product-tool/NUDAPT_44_Documentation.pdf.

Gutiérrez, E., J. E. González, A. Martilli, R. Bornstein, and M. Arend, 2015: Simulations of a heat-wave event in New York City using a multilayer urban parameterization. *J. Appl. Meteor. Climatol.*, **54**, 283–301, https://doi.org/10.1175/JAMC-D-14-0028.1.

Hart, M. A., and D. J. Sailor, 2009: Quantifying the influence of land-use and surface characteristics on spatial variability in the urban heat island. *Theor. Appl. Climatol.*, **95**, 397–406, https://doi.org/10.1007/S00704-008-0017-5.

Heckert, M., and J. Mennis, 2012: The economic impact of greening urban vacant land: A spatial difference-in-differences analysis. *Environ. Plann.*, **44A**, 3010–3027, https://doi.org/10.1068/A4595.

Homer, C., and Coauthors, 2015: Completion of the 2011 National Land Cover Database for the conterminous United

States—Representing a decade of land cover change information. *Photogramm. Eng. Remote Sens.*, **81**, 346–354, https://doi.org/10.14358/PERS.81.5.345.

Hong, S.-Y., J. Dudhia, and S.-H. Chen, 2004: A revised approach to ice microphysical processes for the bulk parameterization of clouds and precipitation. *Mon. Wea. Rev.*, **132**, 103–120, https://doi.org/10.1175/1520-0493(2004)132<0103:ARATIM>2.0.CO;2.

——, Y. Noh, and J. Dudhia, 2006: A new vertical diffusion package with an explicit treatment of entrainment processes. *Mon. Wea. Rev.*, **134**, 2318–2341, https://doi.org/10.1175/MWR3199.1.

Iacono, M. J., J. S. Delamere, E. J. Mlawer, M. W. Shephard, S. A. Clough, and W. D. Collins, 2008: Radiative forcing by long-lived greenhouse gases: Calculations with the AER radiative transfer models. *J. Geophys. Res.*, **113**, D13103, https://doi.org/10.1029/2008JD009944.

Imhoff, M. L., P. Zhang, R. E. Wolfe, and L. Bounoua, 2010: Remote sensing of the urban heat island effect across biomes in the continental USA. *Remote Sens. Environ.*, **114**, 504–513, https://doi.org/10.1016/J.RSE.2009.10.008.

IPCC, 2014: *Climate Change 2014: Impacts, Adaptation, and Vulnerability. Part A: Global and Sectoral Aspects*. C. B. Field et al., Eds., Cambridge University Press, 1132 pp., https://www.ipcc.ch/site/assets/uploads/2018/02/WGIIAR5-PartA_FINAL.pdf.

Janjić, Z. I., 1994: The step-mountain eta coordinate model: Further developments of the convection, viscous sublayer, and turbulence closure schemes. *Mon. Wea. Rev.*, **122**, 927–945, https://doi.org/10.1175/1520-0493(1994)122<0927:TSMECM>2.0.CO;2.

Jones, T. S., M. Liang, M. Kilbourne, M. Griffin, H. D. Donnell Jr., and S. B. Thacker, 1982: Morbidity and mortality associated with the July 1980 heat wave in St Louis and Kansas City, MO. *JAMA*, **247**, 3327–3331, https://doi.org/10.1001/JAMA.1982.03320490025030.

Kain, J. S., 2004: The Kain–Fritsch convective parameterization: An update. *J. Appl. Meteor.*, **43**, 170–181, https://doi.org/10.1175/1520-0450(2004)043<0170:TKCPAU>2.0.CO;2.

Kusaka, H., H. Kondo, Y. Kikegawa, and F. Kimura, 2001: A simple single-layer urban canopy model for atmospheric models: Comparison with multi-layer and slab models. *Bound.-Layer Meteor.*, **101**, 329–358, https://doi.org/10.1023/A:1019207923078.

L'Heureux, M.-A., 2015: The creative class, urban boosters, and race: Shaping urban revitalization in Kansas City, Missouri. *J. Urban Hist.*, **41**, 245–260, https://doi.org/10.1177/0096144214563504.

Li, X.-X., and L. K. Norford, 2016: Evaluation of cool roof and vegetations in mitigating urban heat island in a tropical city, Singapore. *Urban Climate*, **16**, 59–74, https://doi.org/10.1016/J.UCLIM.2015.12.002.

Martilli, A., A. Clappier, and M. W. Rotach, 2002: An urban surface exchange parameterisation for mesoscale models. *Bound.-Layer Meteor.*, **104**, 261–304, https://doi.org/10.1023/A:1016099921195.

Meerow, S., and J. P. Newell, 2017: Spatial planning for multifunctional green infrastructure: Growing resilience in Detroit. *Landscape. Urban Plann.*, **159**, 62–75, https://doi.org/10.1016/J.LANDURBPLAN.2016.10.005.

Mid-America Regional Council, 2013: Troost corridor redevelopment plan: A plan for a sustainable Troost Avenue. MARC Rep., 115 pp., https://www.marc.org/Regional-Planning/pdf/TroostCorridorFinalReport.aspx.

Monaghan, A. J., L. Hu, N. A. Brunsell, M. Barlage, and O. V. Wilhelmi, 2014: Evaluating the impact of urban morphology configurations on the accuracy of urban canopy model temperature simulations with MODIS. *J. Geophys. Res. Atmos.*, **119**, 6376–6392, https://doi.org/10.1002/2013JD021227.

Morini, E., A. G. Touchaei, B. Castellani, F. Rossi, and F. Cotana, 2016: The impact of albedo increase to mitigate the urban heat island in Terni (Italy) using the WRF Model. *Sustainability*, **8**, 999, https://doi.org/10.3390/SU8100999.

Murage, P., S. Hajat, and R. S. Kovats, 2017: Effect of night-time temperatures on cause and age-specific mortality in London. *Environ. Epidemiol.*, **1**, e005, https://doi.org/10.1097/EE9.0000000000000005.

Niyogi, D., K. K. Osuri, N. Busireddy, and R. Nadimpalli, 2020: Timing of rainfall occurrence altered by urban sprawl. *Urban Climate*, **33**, 100643, https://doi.org/10.1016/j.uclim.2020.100643.

Oke, T., 1982: The energetic basis of the urban heat island. *Quart. J. Roy. Meteor. Soc.*, **108**, 1–24, https://doi.org/10.1256/SMSQJ.45501.

——, 1988: The urban energy balance. *Prog. Phys. Geogr.*, **12**, 471–508, https://doi.org/10.1177/030913338801200401.

——, 1995: The heat island of the urban boundary layer: Characteristics, causes and effects. *Wind Climate in Cities*, Springer, 81–107.

Oliveira, S., H. Andrade, and T. Vaz, 2011: The cooling effect of green spaces as a contribution to the mitigation of urban heat: A case study in Lisbon. *Build. Environ.*, **46**, 2186–2194, https://doi.org/10.1016/j.buildenv.2011.04.034.

Pagano, M. A., and A. O. Bowman, 2000: Vacant land in cities: An urban resource. Center on Urban and Metropolitan Policy Rep., 9 pp., https://www.brookings.edu/wp-content/uploads/2016/06/paganofinal.pdf.

Papangelis, G., M. Tombrou, A. Dandou, and T. Kontos, 2012: An urban "green planning" approach utilizing the Weather Research and Forecasting (WRF) modeling system. A case study of Athens, Greece. *Landscape Urban Plann.*, **105**, 174–183, https://doi.org/10.1016/j.landurbplan.2011.12.014.

Peng, S., and Coauthors, 2011: Surface urban heat island across 419 global big cities. *Environ. Sci. Technol.*, **46**, 696–703, https://doi.org/10.1021/es2030438.

Randolph, J., 2012: *Environmental Land Use Planning and Management*. Island Press, 746 pp.

Revi, A., and Coauthors, 2014: Urban areas. *Climate Change 2014: Impacts, Adaptation, and Vulnerability, Part A: Global and Sectoral Aspects*, C. B. Field et al., Eds., Cambridge University Press, 535–612, https://www.ipcc.ch/site/assets/uploads/2018/02/WGIIAR5-Chap8_FINAL.pdf.

Salamanca, F., A. Krpo, A. Martilli, and A. Clappier, 2010: A new building energy model coupled with an urban canopy parameterization for urban climate simulations—Part I. Formulation, verification, and sensitivity analysis of the model. *Theor. Appl. Climatol.*, **99**, 331–344, https://doi.org/10.1007/s00704-009-0142-9.

——, A. Martilli, and C. Yagüe, 2012: A numerical study of the urban heat island over Madrid during the DESIREX (2008) campaign with WRF and an evaluation of simple mitigation strategies. *Int. J. Climatol.*, **32**, 2372–2386, https://doi.org/10.1002/joc.3398.

——, M. Georgescu, A. Mahalov, M. Moustaoui, and M. Wang, 2014: Anthropogenic heating of the urban environment due to air conditioning. *J. Geophys. Res. Atmos.*, **119**, 5949–5965, https://doi.org/10.1002/2013JD021225.

Santamouris, M., 2013: Using cool pavements as a mitigation strategy to fight urban heat island—A review of the actual developments. *Renewable Sustainable Energy Rev.*, **26**, 224–240, https://doi.org/10.1016/j.rser.2013.05.047.

——, 2014: Cooling the cities—A review of reflective and green roof mitigation technologies to fight heat island and improve comfort in urban environments. *Sol. Energy*, **103**, 682–703, https://doi.org/10.1016/j.solener.2012.07.003.

Schilling, J., and J. Logan, 2008: Greening the Rust Belt: A green infrastructure model for right sizing America's shrinking cities. *J. Amer. Plann. Assoc.*, **74**, 451–466, https://doi.org/10.1080/01944360802354956.

Shahmohamadi, P., A. Che-Ani, K. Maulud, N. Tawil, and N. Abdullah, 2011: The impact of anthropogenic heat on formation of urban heat island and energy consumption balance. *Urban Stud. Res.*, **2011**, 497524, https://doi.org/10.1155/2011/497524.

Shepherd, J. M., 2005: A review of current investigations of urban-induced rainfall and recommendations for the future. *Earth Interact.*, **9**, https://doi.org/10.1175/EI156.1.

Skamarock, W. C., J. B. Klemp, J. Dudhia, D. O. Gill, D. M. Barker, W. Wang, and J. G. Powers, 2005: A description of the Advanced Research WRF version 2. NCAR Tech. Note NCAR/TN-468+STR, 88 pp., http://doi.org/10.5065/D6DZ069T.

Stone, B., 2012: *The City and the Coming Climate: Climate Change in the Places We Live*. Cambridge University Press, 187 pp.

Susca, T., S. R. Gaffin, and G. Dell'Osso, 2011: Positive effects of vegetation: Urban heat island and green roofs. *Environ. Pollut.*, **159**, 2119–2126, https://doi.org/10.1016/j.envpol.2011.03.007.

Taha, H., 1997: Urban climates and heat islands: Albedo, evapotranspiration, and anthropogenic heat. *Energy Build.*, **25**, 99–103, https://doi.org/10.1016/S0378-7788(96)00999-1.

Takebayashi, H., and M. Moriyama, 2007: Surface heat budget on green roof and high reflection roof for mitigation of urban heat island. *Build. Environ.*, **42**, 2971–2979, https://doi.org/10.1016/j.buildenv.2006.06.017.

Tan, J., and Coauthors, 2010: The urban heat island and its impact on heat waves and human health in Shanghai. *Int. J. Biometeor.*, **54**, 75–84, https://doi.org/10.1007/s00484-009-0256-x.

Tewari, M., and Coauthors, 2004: Implementation and verification of the unified Noah land surface model in the WRF Model. *20th Conf. on Weather Analysis and Forecasting/16th Conf. on Numerical Weather Prediction*, Seattle, WA, Amer. Meteor. Soc., 14.2A, https://ams.confex.com/ams/pdfpapers/69061.pdf.

Tran, H., D. Uchihama, S. Ochi, and Y. Yasuoka, 2006: Assessment with satellite data of the urban heat island effects in Asian mega cities. *Int. J. Appl. Earth Obs. Geoinf.*, **8**, 34–48, https://doi.org/10.1016/j.jag.2005.05.003.

U.S. Census Bureau, 2011: Population change for metropolitan and micropolitan statistical areas in the United States and Puerto Rico: 2000 to 2010 (CPH-T-2). U.S. Census Bureau, https://www.census.gov/data/tables/time-series/dec/cph-series/cph-t/cph-t-2.html.

——, 2018: Annual estimates of the resident population: April 1, 2010 to July 1, 2017, United States metropolitan statistical area; and for Puerto Rico, 2017 population estimates. U.S. Census Bureau, https://www.wpr.org/sites/default/files/RK census report.pdf.

Voogt, J., 2007: How researchers measure urban heat islands. U.S. Environmental Protection Agency Presentation Material, 34 pp., https://19january2017snapshot.epa.gov/sites/production/files/2014-07/documents/epa_how_to_measure_a_uhi.pdf.

Wesley, E. J., and N. A. Brunsell, 2019: Greenspace pattern and the surface urban heat island: A biophysically-based approach to investigating the effects of urban landscape configuration. *Remote Sens.*, **11**, 2320–2322, https://doi.org/10.3390/rs11192322.

Yang, L., D. Niyogi, M. Tewari, D. Aliaga, F. Chen, F. Tian, and G. Ni, 2016: Contrasting impacts of urban forms on the future thermal environment: Example of Beijing metropolitan area. *Environ. Res. Lett.*, **11**, 034018, https://doi.org/10.1088/1748-9326/11/3/034018.

Zhou, Y., and J. M. Shepherd, 2010: Atlanta's urban heat island under extreme heat conditions and potential mitigation strategies. *Nat. Hazards*, **52**, 639–668, https://doi.org/10.1007/s11069-009-9406-z.